Oxidation of 9CrODS Exposed to Supercritical Water

J. Bischoff and A.T. Motta
Department of Mechanical and Nuclear Engineering, 227 Reber Building, Pennsylvania State University, University Park, PA, 16802.
Contact: jbb236@psu.edu

Y. Chen and T.R.Allen
Department of Engineering Physics, 3335 Engineering Hall, 1415 Engineering Drive, University of Wisconsin, Madison, WI, 53706

ABSTRACT

The oxide layers formed on 9CrODS have been characterized using synchrotron radiation fluorescence and diffraction. This analysis showed a three-layer structure with an outer layer containing only Fe_3O_4, an inner layer containing a mixture of $FeCr_2O_4$ and Fe_3O_4, and a diffusion layer containing a mixture of metal grains and $FeCr_2O_4$ precipitates. A Cr_2O_3 ribbon formed at the diffusion layer-metal interface on the samples exposed to 600ºC supercritical water for 4 and 6 weeks. Calculations of the oxidation behavior were undertaken to calculate the activation energy and the corrosion rate constant *n* of power law kinetics. These calculations showed that the oxidation behavior of this alloy could not be described by a power law because the oxide microstructure changes with exposure time and those between the samples exposed to 500ºC and to 600ºC. Additionally, the outward flow of iron was calculated and showed that not enough iron migrates outwards to be able to form the outer layer suggesting that other mechanisms might be at work. Finally, a qualitative description of the oxidation behavior of 9CrODS is displayed showing the importance of the role played by Cr_2O_3 in the corrosion process.

Key words: corrosion, supercritical water, oxide dispersion strengthened steel, oxidation

INTRODUCTION

The Supercritical Water Reactor (SCWR) is one of the Generation IV power plant designs envisioned for its high thermal efficiency and simplified core. One of the major materials issues for the development of this reactor is the corrosion resistance of the cladding and structural materials exposed to supercritical water at a temperature between 500ºC and 600ºC, and at a pressure of about 25 MPa [1].

A promising material for such an application, 9CrODS, is an oxide dispersion strengthened steel containing yttrium-rich oxide nano-particles, and was initially developed by Japan Atomic Energy Agency for application in sodium cooled fast reactors [2, 3]. The alloy's higher creep strength and radiation damage resistance make it a very good candidate for the supercritical water reactor. Additionally, 9CrODS exhibits good corrosion resistance which has been attributed to the segregation at the grain boundaries of chromium (forming Cr_2O_3) and yttrium from the yttrium-rich oxide nano-particles [4, 5]. It appears as if the yttrium segregation plays an active role in the formation of chromium rich phases at the grain boundaries [4].

In a previous study we have shown the results of the characterization of oxide layers formed on 9CrODS after exposure to supercritical water at 500ºC and 600ºC for 2, 4 and 6 weeks [6]. Synchrotron radiation X-ray diffraction and fluorescence coupled with scanning electron microscopy (SEM) were used for this characterization. A complementary study focused on transmission electron microscopy (TEM) analysis of the oxide layers formed on 9CrODS [7]. In this article, we will briefly summarize those results and use these results as a basis for calculations concerning the corrosion behavior of the alloy and for qualitative description of the oxidation behavior of 9CrODS.

CHARACTERIZATION OF THE OXIDE LAYER

All the results in this section were described in detail in a previous article and are reviewed here to instruct on the corrosion behavior [6]. Figure 1 shows SEM images and X-ray fluorescence data from the 9CrODS samples exposed to 600ºC supercritical water for 2, 4 and 6 weeks. The SEM images reveal a three-layer oxide structure. The X-ray diffraction data show that the outer layer is composed of Fe_3O_4, that the inner layer contains a mixture of Fe_3O_4, $FeCr_2O_4$, and Cr_2O_3, and that the diffusion layer contains $FeCr_2O_4$ and a Cr_2O_3 ribbon at the diffusion layer-metal interface.

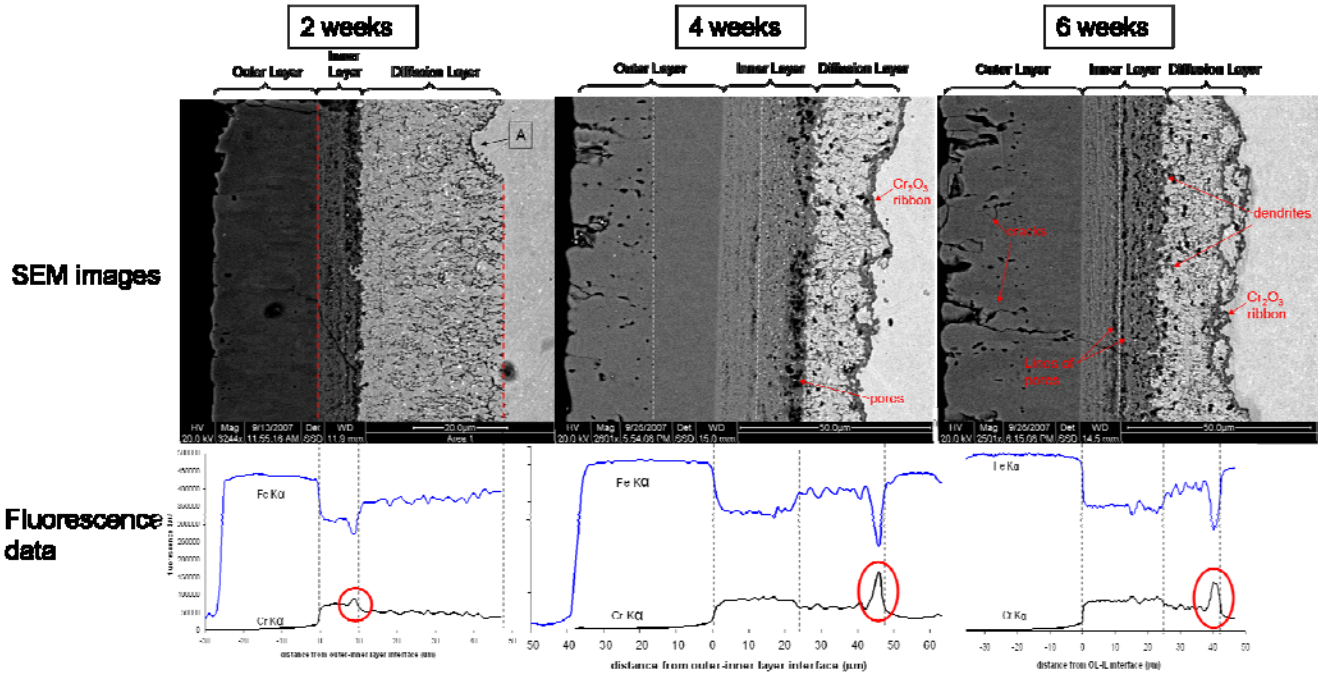

FIGURE 1 - SEM images and X-Ray fluorescence data of the oxide layers formed on 9CrODS exposed to 600ºC supercritical water for 2, 4 and 6 weeks [6].

In the 600ºC 2-week sample, the diffusion layer is much larger than the inner layer and ends in a distinct line at the diffusion layer-metal interface. The well defined diffusion layer-metal interface is thought to correspond to the location where the solubility limit of oxygen in the metal is reached, causing oxide precipitation. The 600ºC 2-week sample also exhibits a porous inner-diffusion layer interface and smaller periodic lines of pores in the inner layer. The fluorescence data shows chromium enrichment at the inner-diffusion layer interface which the diffraction data show is associated with the presence of Cr_2O_3.

In the 600ºC 4-week sample, a ribbon has appeared at the diffusion layer-metal interface. Diffraction analysis shows this ribbon is constituted mainly of Cr_2O_3. TEM analysis has shown that this ribbon forms a continuous Cr_2O_3 layer containing very few iron "islands" [7]. No oxide particles are observed in the metal beyond this ribbon. Thus, this ribbon appears to almost stop the advancement of the oxide into the metal. Additionally, the porosity present at the inner-diffusion layer interface is higher than in the 2-week sample and porosity also appears both in the diffusion layer and in the outward portion of the outer layer. Finally, the fluorescence data show a shift in the chromium enrichment from the inner-diffusion layer interface for the 2-week sample to the diffusion layer-metal interface for the 4- and 6-week samples. Both in the 4-and 6-week samples, the chromium enrichment is associated with the presence of Cr_2O_3.

The 600ºC 6-week sample exhibits a similar structure to that of the 4-week sample except that the thick line of pores present at the inner-diffusion layer interface in the 4-week sample is more spread out and thin lines of pores are present in the middle of the inner layer. Additionally, the outer layer appears to be more porous in its outer region than that of the 4-week sample.

Other 9CrODS samples were exposed to 500ºC supercritical water for 2, 4 and 6 weeks. The SEM images of these three samples, shown in Figure 2, reveal a dual-layer structure, suggesting that the oxidation behavior at 500ºC is different from that at 600ºC. Nevertheless a diffusion layer can be discerned in the SEM images by difference in contrast in the region of the metal adjacent to the oxide. Very little oxide precipitation is observed in that diffusion layer, which suggests that the diffusion layer may be a solid solution of oxygen ahead of the oxide. In the 6-week sample, the diffusion layer is visible and has a similar appearance to the inner layer but has a slightly lighter contrast. Furthermore, in the 500ºC 6-week sample we observe that oxide precipitates form at metal grain boundaries before oxidizing the inside of the grain. The diffraction data show that both the inner and the outer layer contain mainly Fe_3O_4 with very small quantities of Cr_2O_3 and $(Fe,Cr)_3O_4$ in the inner layer. $FeCr_2O_4$ is observed at the outer-inner oxide interface. Additionally, the body centered cubic iron metal is observed throughout the inner layer with decreasing intensity from the metal to the outer layer. This suggests that the metal is not yet completely oxidized in the inner layer. This hypothesis is consistent with the presence of light spots in the inner layer shown in the SEM images.

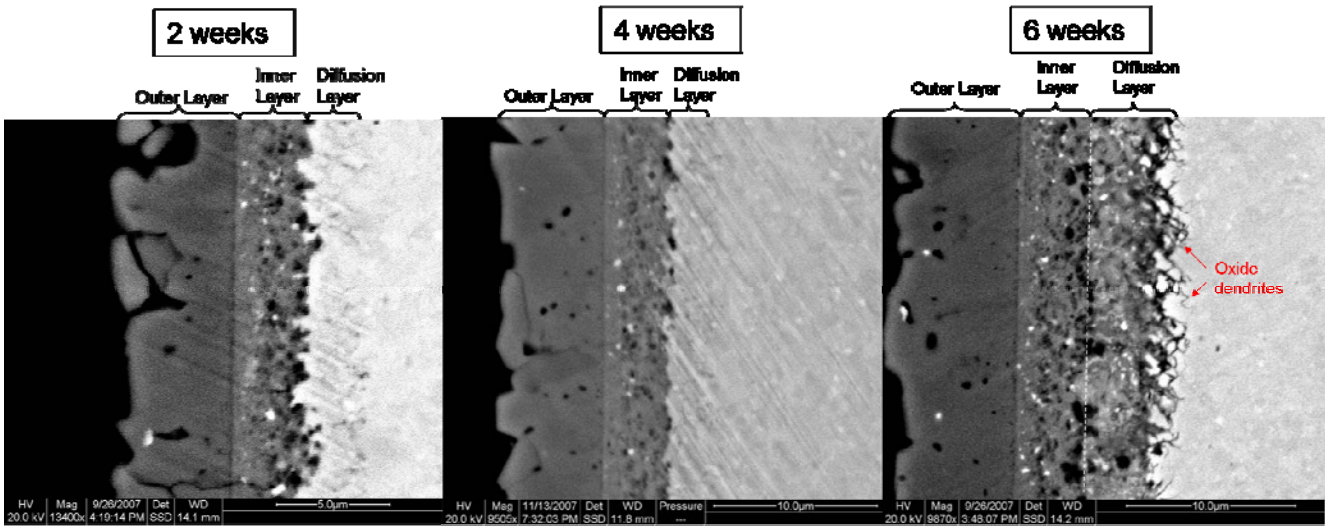

FIGURE 2 - SEM images of 9CrODS oxide layers formed during exposure to supercritical water at 500ºC for 2, 4 and 6 weeks [6].

CALCULATIONS

Oxidation behavior calculations:

Most studies of the oxidation behavior of ferritic-martensitic steels use weight gain as a measure of the corrosion rate of the alloy [4, 5, 8-11]. Nevertheless, this method may not be the most appropriate, since there is evidence that i) the outer layer spalls off and ii) that a diffusion layer containing oxygen is present. Both of these phenomena make the relationship between the oxide layer thickness and the weight gain more difficult to assess. Since the corrosion rate calculations were derived for the oxide thickness and then transposed to weight gain measurements, it seems more appropriate to measure the corrosion rate by using oxide thicknesses. Additionally, the use of weight gain measurements does not take into account the variations in oxide structure as observed between the 9CrODS 600ºC 2-and 4-week samples for example. Consequently, throughout this article we will use oxide thicknesses to measure the corrosion rate. The diffusion layer will not be considered in the measurement of the oxide thicknesses since it is mostly composed of the base metal with few oxide precipitates.

The corrosion rate is commonly expressed by the formula shown in Equation 1:

$$L = (k.t)^{1/n} \tag{1}$$

where L is the oxide thickness, k is a constant, t is time, and n is the exponent describing the time dependence of the oxidation. In this equation, the constant k is a function of temperature (T) as follows [11] :

$$k = k_0 \exp\left(-\frac{Q}{RT}\right) \tag{2}$$

where Q is the activation energy of the rate limiting step in the corrosion reaction and k_0 a constant.

It is possible to determine n and k using the overall oxide thickness (sum of the outer and inner layer thicknesses) or to use the thickness thought to be related to the rate-limiting step, for example the inner layer thickness. There is evidence supporting this second choice as the diffusion of iron and

oxygen through chromium-rich oxides (and especially a film of Cr_2O_3) have been shown to be much slower than in Fe_3O_4 [12, 13]. Consequently, we will plot both quantities as a function of the overall oxide thickness and as a function of the inner layer thickness.

To calculate the time dependence constant *n* the logarithm of the thickness, in μm, is plotted as a function of the logarithm of the exposure time, in hours. If the oxidation rate follows equation 1 then we should obtain a linear plot in which the slope corresponds to *1/n*. Since 9CrODS was oxidized at both 500ºC and 600ºC we calculated the value of *n* for these two temperatures. Table 1 summarizes values used for the plots with the oxide thicknesses and times for the two temperatures. The oxide thicknesses were measured as an average from the SEM images.

TABLE 1

Oxide layer thicknesses (μm) formed on 9CrODS after exposure to supercritical water at 500ºC and 600ºC during 2, 4 and 6 weeks.

	2 weeks	4 weeks	6 weeks
500C	**336 h**	**690 h**	**1026 h**
inner layer	3.5	4	4.3
outer layer	4.8	6.5	7
600C	**333 h**	**667 h**	**1000 h**
inner layer	10	23	24
outer layer	22	38	39

Figure 3 shows the log-log plots of oxide thickness (inner layer or total thickness) versus exposure time.

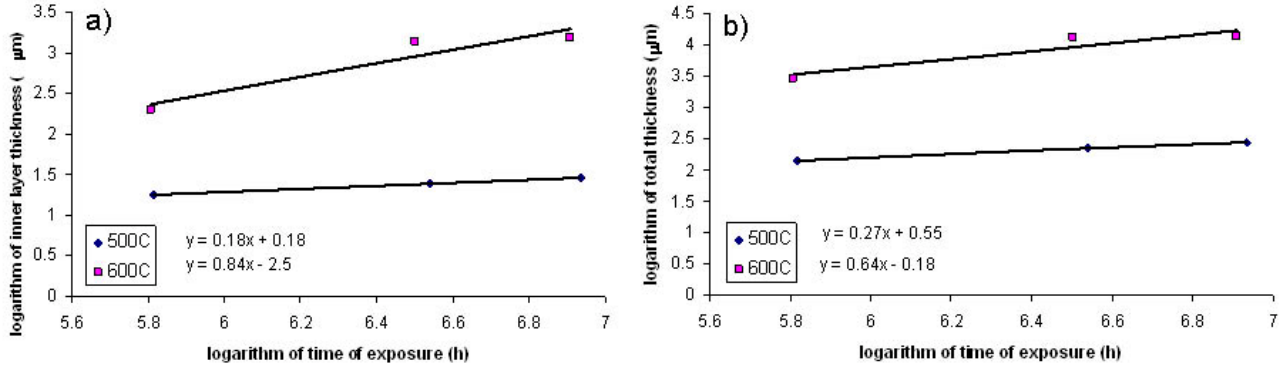

FIGURE 3 - Plot of the logarithm of the oxide thickness as a function of the logarithm of the exposure time. a) corresponds to the plot using only the inner layer thickness; b) uses the sum of the inner and outer layer thicknesses.

The slopes of the curves plotted in Figure 3 correspond to *1/n*. In the plot using only the inner layer thickness, we obtain values of *n = 5.4* at 500ºC and *n = 1.2* at 600ºC. In the plot using the whole oxide layer thickness, the values obtained were *n = 3.7* at 500ºC and *n = 1.6*. In both cases, there is a large difference between the 500ºC and 600ºC values, which suggests that the oxidation mechanism is different at these two temperatures. This hypothesis is coherent with the different oxide structure observed in the SEM images in Figures 1 and 2 and consistent with the lower oxide density observed at 600ºC [5]. If the corrosion mechanism at 500ºC and 600ºC are different, the activation energy at these two temperatures should be different and therefore it is impossible for us to calculate the activation energy. Additionally, if we only consider the samples corroded at 600ºC, it would seem as if we should

get different activation energies for the 2-week sample compared to the 4 and 6 week samples since the Cr_2O_3 ribbon appears between 2 and 4 weeks and almost stops further diffusion of oxygen beyond the ribbon. In the same way, the log-log plot for the calculation of *n* shown in Figure 3 are not valid for the 600ºC and thus give non-physical values, because the Cr_2O_3 ribbon has formed between the 2-and 4-week samples thus changing the corrosion kinetics. When considering only the 4-and 6-week points, the value of *n* is very close to zero. In this respect, the Cr_2O_3 ribbon could be the barrier layer.

The fact that different values of *n* are calculated from the data at 500ºC and 600ºC would indicate that different corrosion mechanisms may be at work as seen previously with zirconium alloys [14]. Furthermore, the fact that the calculated values of *k* and *n* using different oxide thicknesses do not agree indicate that it may not be possible to derive a simple description of the corrosion process in these alloys as would be obtained using equation 1 and 2. This makes us question the validity of the procedure of obtaining *k* and *n*.

Calculations of the outward flow of iron ions:

Since it appears clear that the outer layer is formed by iron migrating outwards, a calculation of the outward flow of iron ions is undertaken. We assume that the chromium does not diffuse out of the inner layer or diffusion layer. Therefore as the oxide layer is formed, iron ions diffusing out of these layers will engender chromium enrichment in these layers, as is observed in the microbeam synchrotron radiation fluorescence data collected at the APS. By measuring the evolution of the chromium to iron ratio it is possible to calculate the quantity of iron that has left the inner layer in order to form the outer layer and compare it with the measurements.

The chromium to iron ratio in the inner layer compared to that in the base metal was measured using the fluorescence data. In order to use this data it is necessary to first ensure that the values measured for the base metal were equivalent to the theoretical value obtained from the elemental composition of the alloy. HCM12A and HT9 were two other alloys studied during this project and were used here to confirm that the fluorescence data could be used as an estimate for the chromium to iron ratio in the calculations. This comparison is shown in Table 2.

TABLE 2

Comparison of the chromium to iron ratio using the synchrotron fluorescence data with the theoretical value calculated from the elemental composition for three alloys studied: HT9, HCM12A and 9CrODS.

sample	Fluorescence data ratio (%)	Theoretical elemental ratio (%)
HT9 500C 1w	14.21	14.15
HCM12A 600C 2w	12.89	12.86
9CrODS 600C 2w	9.83	9.78

The values calculated using the fluorescence data are similar to the theoretical elemental ratio calculated using the concentration of the alloying elements. Consequently, the fluorescence data can be used to estimate the outward flow of iron. In this calculation, we will consider the iron migration not only from the inner layer but also from the diffusion layer and the chromium enrichment peak located at the inner-diffusion layer interface in the 9CrODS 600ºC 2-week sample and at the diffusion layer-metal interface in the 9CrODS 600ºC 4-and 6-week samples.

The balance of iron ions can thus be written:

$$n_{Fe_{OL}} = n_{Fe_{ini}} - n_{Fe_{IL}} \tag{3}$$

In Equation 3, $n_{Fe_{OL}}$ represents the amount of iron ions used to form the outer layer, $n_{Fe_{ini}}$ the initial iron content in the inner layer before oxidation, and $n_{Fe_{IL}}$ the iron content in the inner layer after oxidation. Using the relation between the number of moles and the thickness for a unit area ($n = \frac{\rho}{M} h$ with ρ the density and *M* the molar mass) we end up with the following equation:

$$\begin{aligned} h_{OL} &= \left(1 - \frac{n_{Fe_{IL}}}{n_{Fe_{ini}}}\right) h_{IL} + \left(1 - \frac{n_{Fe_{DL}}}{n_{Fe_{ini}}}\right) h_{DL} + \left(1 - \frac{n_{Fe_{enricht}}}{n_{Fe_{ini}}}\right) h_{enrich} \\ h_{OL} &= \left(1 - \frac{\alpha_{ini}}{\alpha_{IL}}\right) h_{IL} + \left(1 - \frac{\alpha_{ini}}{\alpha_{DL}}\right) h_{DL} + \left(1 - \frac{\alpha_{ini}}{\alpha_{enrich}}\right) h_{enrich} \end{aligned} \tag{4}$$

In Equation 4, $\alpha_{ini} = \frac{n_{Cr}}{n_{Fe_{ini}}}$, $\alpha_{IL} = \frac{n_{Cr}}{n_{Fe_{IL}}}$, $\alpha_{DL} = \frac{n_{Cr}}{n_{Fe_{DL}}}$ and $\alpha_{enrich} = \frac{n_{Cr}}{n_{Fe_{enrich}}}$. Using the values measured for the inner layer thickness and the chromium to iron concentration ratios we calculated the resulting outer layer thickness and compared it to the measured outer layer thickness. For all the calculations we used $\alpha_{ini} = 9.78\%$. The results are shown in Table 3.

TABLE 3
Comparison of the outer layer thickness calculated using the concentration of iron that has migrated outwards compared to the measured value

sample	α_{IL} (%)	α_{DL} (%)	α_{enrich} (%)	h_{IL} (µm)	h_{OL} (µm)	measured OL thickness (µm)
9CrODS 600 2w	23	14	33	10	17.3	22
9CrODS 600 4w	25	15.5	46	23	26.1	38
9CrODS 600 6w	25	17	48	24	27	38
9CrODS 500 4w	22.3	12.3	N/A	4	3.1	6.5
9CrODS 500 6w	22.5	12.5	N/A	4.3	3.3	7

The results of Table 3 show that the amount of iron needed to form the outer layer is larger than the amount that migrates outwards from the inner layer, diffusion layer and chromium enrichment region. This result suggests that the outer layer formation cannot be described by simple outward migration of iron from the inner and diffusion layers. The fact that the calculated outer layer thickness for the 500ºC samples is smaller than the inner layer suggests there may be an additional mechanism at work since we always observe a larger outer layer. Consequently, the oxidation behavior of this alloy appears complex and cannot be described through simple calculations.

QUALITATIVE OXIDATION BEHAVIOR

Several models have been developed to try to describe the corrosion behavior of chromium rich steel alloys. For example, Wagner's theory describes in a simple way the oxidation of a metal by diffusion process trough a single homogeneous layer [15]. Later on, Whittle and Wood used the difference of diffusion coefficients between chromium and iron to elaborate a stratified scale model [16]. At about the same time, Robertson suggested that the oxygen was migrating inwards in the form of water molecules to reach the oxide-metal interface through nano-pores [17]. Overall, these models are not applicable to our case since they do not explain or consider the formation of a diffusion layer, and it is assumed in these models that the oxide layers are homogeneous and uniform. From the characterization of the oxide structure of 9CrODS reviewed at the beginning of this article and described in a previous article [6], we have seen that the oxide layers contain different phases located in certain regions. Consequently, we will go over a qualitative description of the oxidation behavior of 9CrODS taking the diffusion layer and the inhomogeneity of the layers into account.

A few critical observations made in the characterization of the oxide layers formed in 9CrODS are reviewed here to motivate the qualitative description [6]. The first observation is that the outer-inner layer interface is quite distinct and straight, which suggests that this interface is the original solution-metal interface prior to oxidation. Furthermore, fluorescence data collected at the APS show that the inner layer is enriched in chromium relative to the chromium content in the metal and the outer layer does not contain any chromium. Moreover, other studies have shown by isotopic analysis that the interfaces of oxide growth are the solution-outer layer interface and the inner-metal interface in a duplex oxide structure [18]. Consequently, the Fe_3O_4 outer layer is formed by outward diffusion of iron and the inner layer is formed by inward diffusion of oxygen.

Additionally, we observed chromium enrichment accompanied by the presence of Cr_2O_3 at the inner-diffusion layer interface for the 9CrODS 600ºC 2-week sample and at the diffusion layer-metal interface for the 9CrODS 600ºC 4-week and 6-week samples. We nevertheless still observed Cr_2O_3 at the inner-diffusion layer interface in the 9CrODS 600ºC 4 week sample but not in the 6 week sample. The Cr_2O_3 present at the inner-diffusion layer interface is part of a mixture of $FeCr_2O_4$ and Cr_2O_3 but a Cr_2O_3 ribbon forms at the diffusion layer-metal interface in the 9CrODS 600ºC 4 and 6 week samples. Over a thickness of a few microns in this ribbon, Cr_2O_3 is the only oxide phase present and this appears to stop oxygen diffusion beyond this ribbon.

Thermodynamics show that Cr_2O_3 is the most stable oxide and is formed at the lowest partial pressure of oxygen, followed by $FeCr_2O_4$ at slightly higher oxygen partial pressures and finally Fe_3O_4 at much higher partial pressures of oxygen [10, 19]. Consequently, Cr_2O_3 and $FeCr_2O_4$ form at low oxygen concentrations while Fe_3O_4 forms at higher oxygen concentrations. The presence of Cr_2O_3 at both the inner-diffusion layer interface and the diffusion layer-metal interface serves both as a kinetic and thermodynamic barrier since the presence of Cr_2O_3 decreases the diffusion coefficients of iron and oxygen but also decreases the oxygen potential at the inner interface of Cr_2O_3 precipitates [13]. It is assumed that the Cr_2O_3 ribbon, where Cr_2O_3 is the only oxide phase formed, stops the diffusion of oxygen beyond the ribbon and also the outward diffusion of iron from the metal towards the oxide. In the same way, $FeCr_2O_4$ slows down the diffusion of both oxygen and iron because of its high chromium concentration but does not stop the diffusion. Additionally, we will assume that chromium diffuses on short distances at 600ºC but not at 500ºC. Figure 4 shows a schematic of a possible oxidation mechanism for 9CrODS.

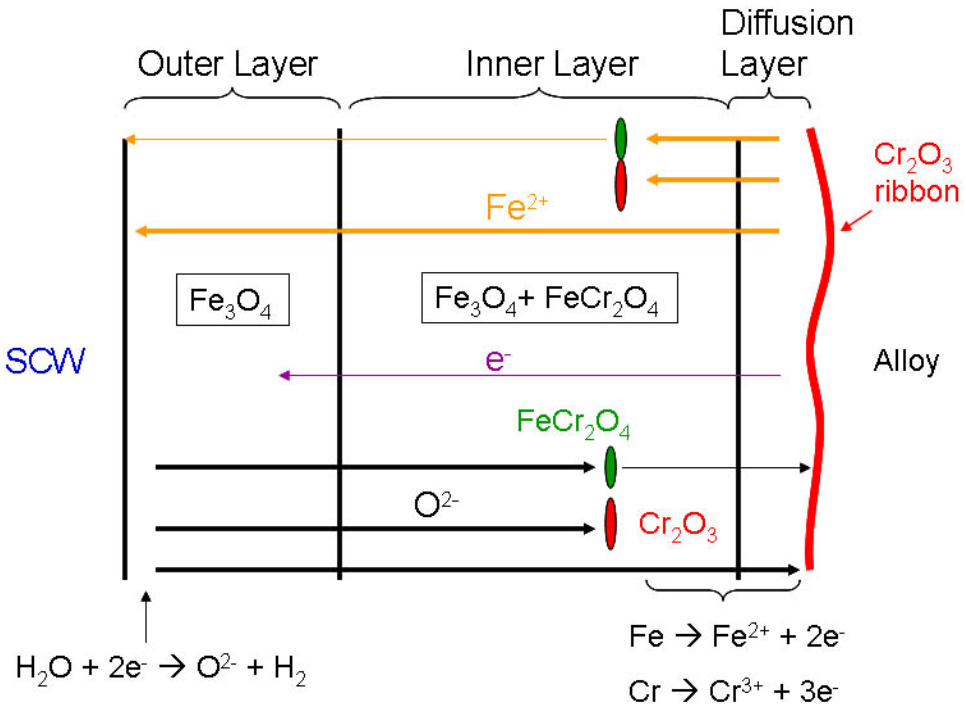

FIGURE 4 - Schematic of the oxidation mechanism of 9CrODS.

Using the basic oxidation behavior mechanism described, we will analyze the evolution with exposure time of the 9CrODS 600ºC samples. Figure 5 shows a schematic of the oxide structure of the 9CrODS 600ºC 2 week sample.

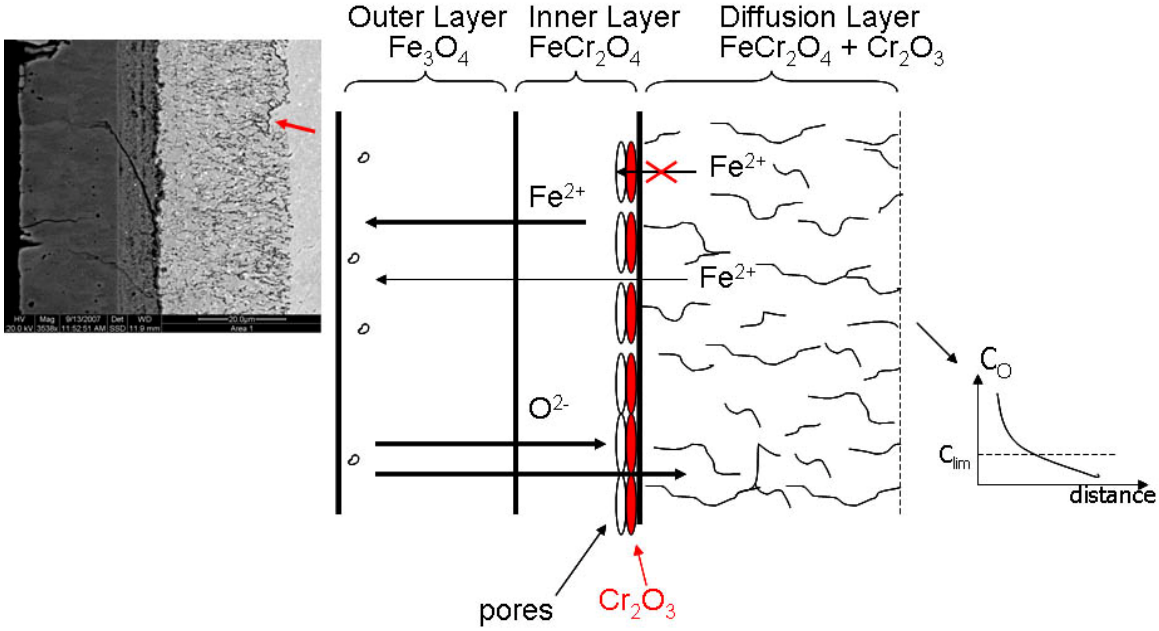

FIGURE 5 - Schematic of the oxidation behavior of 9CrODS 600ºC 2 weeks.

This sample is characterized by chromium enrichment and Cr_2O_3 observed in a relatively large quantity at the inner-diffusion layer interface. Additionally, lines of pores are found at this interface as well. Consequently, it appears that the presence of Cr_2O_3 slows down the oxidation of iron in the

diffusion layer and hinders the outward migration of iron ions towards the outer layer. The iron needed to form the outer layer is thus taken from the inner layer, thus creating vacancies that coalesce into pores. The pores remain at the inner-diffusion layer interface because the presence of Cr_2O_3 hinders the replenishment of the vacancies and pores by the outward diffusion of iron ions from the diffusion layer.

Additionally, the Cr_2O_3 present at the inner-diffusion layer interface does not form a continuous film of only Cr_2O_3 but is mixed with $FeCr_2O_4$ and remains of iron body-centered cubic grains that are not yet fully oxidized. Consequently, oxygen is able to diffuse through this interface but in a much smaller quantity forming $FeCr_2O_4$ dendritic oxide precipitates in the diffusion layer. The large diffusion layer ends in a relatively straight line at the diffusion layer-metal interface. This interface is a line because an oxygen solubility limit exists in the metal below which precipitation of oxides cannot occur. Additionally, we can observe the beginning of formation of the Cr_2O_3 ribbon at the diffusion layer-metal interface in the top right corner of the SEM image, shown by the red arrow in Figure 5. The formation of this ribbon is not yet elucidated but the local migration of chromium is likely to play a role in this formation. Figure 6 shows the schematic of the oxidation process for 9CrODS 600ºC 4 weeks.

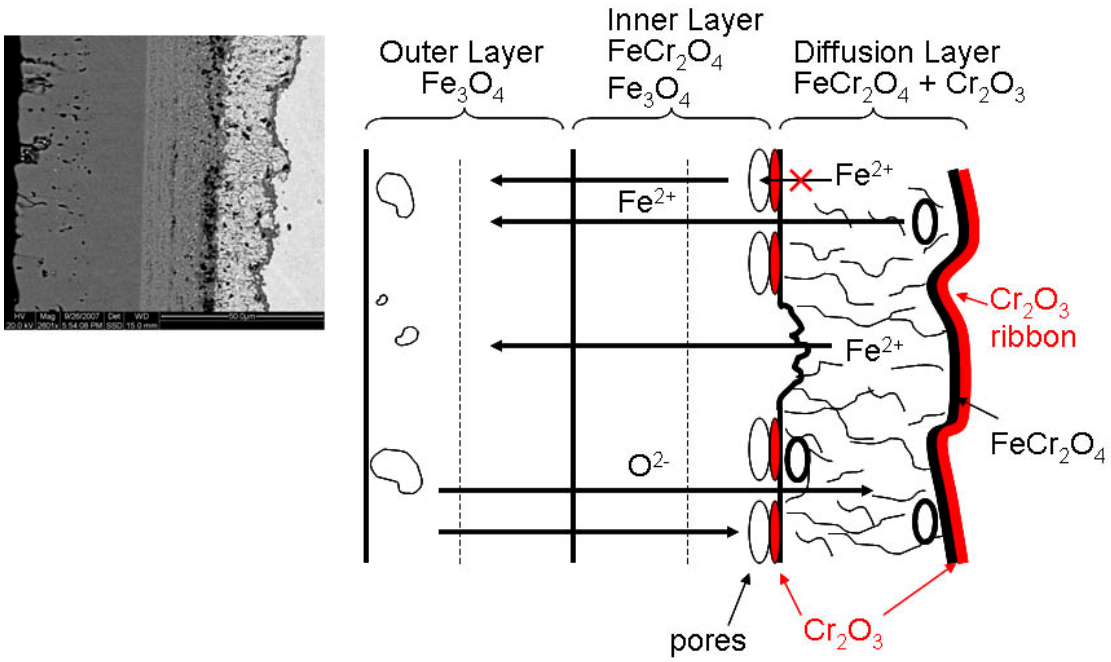

FIGURE 6 - Schematic of the oxidation behavior for 9CrODS 600ºC 4 weeks.

In the 9CrODS 600ºC 4-week sample, a uniform ribbon of Cr_2O_3 ribbon has formed. Consequently, the diffusion of oxygen is stopped by this barrier layer. Henceforth, the thickness ratio of the inner oxide over the diffusion layer thickness has increased during the 2 week to the 4 week sample from about 0.33 to 0.5. Just behind the Cr_2O_3 ribbon a film of $FeCr_2O_4$ is observed which is due to the higher oxygen concentration in the part of the ribbon near the diffusion.

Additionally, the pores at the inner-diffusion layer interface are larger than in the 2 week sample, suggesting that more iron from the inner layer diffused towards the outer layer but not enough iron was oxidized to replenish the pores, and that most of the iron needed for the formation of the outer layer came from the inner layer. Nevertheless, the oxidation of the metal present in the diffusion layer is also taking place since pores are observed in the diffusion layer. In the SEM image shown in Figure 6, a region of the inner-diffusion layer interface does not exhibit pores, and in this region the inner layer

advances into the diffusion layer. This is probably due to the disappearance of the Cr_2O_3 at the interface in this region thus enabling more oxidation of the diffusion layer which creates Fe^{2+} that can replenish the pores.

This disappearance of the Cr_2O_3 at the inner-diffusion layer interface that was observed in one region of the 9CrODS 600ºC 4-week sample has happened throughout the interface in the 9CrODS 600ºC 6-week sample. Consequently, the pores are spread out over the whole inner half of the inner layer. Figure 7 shows the schematic of the oxidation behavior for 9CrODS 600ºC 6 weeks.

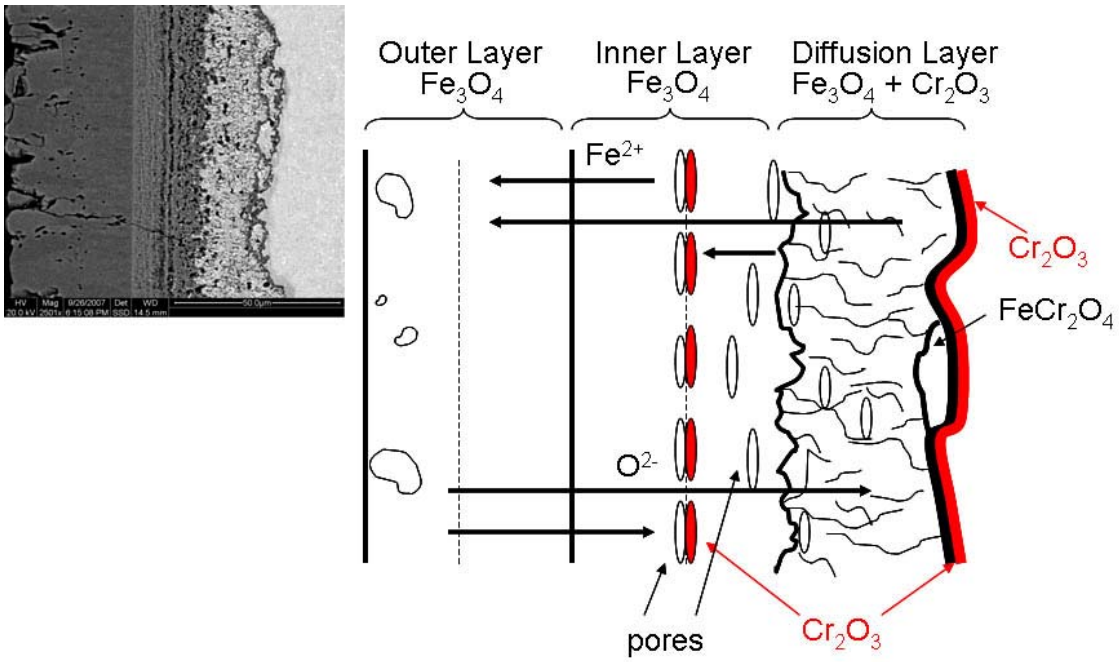

FIGURE 7 - Schematic of the oxidation behavior for 9CrODS 600ºC 6 weeks.

Although the oxide structure observed for the 6-week sample is very similar to the one observed for the 4 week sample, it differs in mainly three aspects. First, Cr_2O_3 at the inner-diffusion layer interface disappears, which enables the inner oxide layer to advance and oxidize the diffusion layer. This phenomenon spreads out the pores throughout the inner half of the inner oxide layer. If this advancement continues it is possible that the inner oxide layer eventually "catches up" with the protective oxide ribbon at the diffusion layer-metal interface. However, no samples were corroded for longer exposure times than 6 weeks, so this hypothesis cannot yet be proven. Cr_2O_3 is observed in the middle of the inner layer where lines of pores are also observed which reinforces the idea of the line of pores being linked to the presence of Cr_2O_3. The question left unanswered is how come the Cr_2O_3 forms in the middle of the inner layer and not at the inner-diffusion layer interface where the oxygen concentration is lower.

Second, very little $FeCr_2O_4$ is observed both in the inner and the diffusion layer. In the diffusion layer we observe $Fe_{1+x}Cr_{2-x}O_4$ and in the inner layer we essentially observe Fe_3O_4. This phase change is likely due to the disappearance of Cr_2O_3 at the inner-diffusion layer interface which enables the oxygen concentration to homogenize over both the inner and diffusion layers, thus enabling the formation of iron rich oxides. It is possible that if the oxygen concentration becomes high enough near the diffusion layer-metal interface, the Cr_2O_3 ribbon will decompose into a less protective oxide containing more iron and thus the metal will be further oxidized until a new Cr_2O_3 ribbon is formed.

Finally, small $FeCr_2O_4$ ribbons have formed near the Cr_2O_3 ribbon in the diffusion layer. These could be due to the coalescence of $FeCr_2O_4$ precipitates present in the diffusion layer or to the Cr_2O_3

ribbon advancing due to an increase in the oxygen concentration in the diffusion layer. The fact that the summation of the inner and diffusion layer thicknesses is approximately equal in the 2, 4 and 6 week samples suggests that these ribbons are formed by the coalescence of precipitates in the diffusion layer, but the other explanation is very plausible.

Concerning the oxidation behavior of 9CrODS exposed to 500ºC supercritical water, the oxide structure is completely different from what is observed at 600ºC. The main reason for this is the low diffusion coefficient of chromium at 500ºC. Consequently, chromium does not diffuse even on short ranges to be oxidized and no Cr_2O_3 is formed because a 14 wt% concentration of chromium is necessary to form Cr_2O_3 and 9CrODS only contains 8.6 wt%. In the same way no precipitation is observed in the diffusion layer and the main phase in the inner layer is Fe_3O_4 instead of being $FeCr_2O_4$ due to low chromium diffusion.

CONCLUSION

The structure of the oxide layers formed on 9CrODS exhibits a three layer structure with an outer layer containing only Fe_3O_4, an inner layer containing a mixture of $FeCr_2O_4$ and Fe_3O_4, and a diffusion layer containing a mixture of metal grains and $FeCr_2O_4$ precipitates. Cr_2O_3 is observed at the inner-diffusion layer interface for the 600ºC 2-and 4-week samples and at the diffusion layer-metal interface for the 600ºC 4-and 6-week samples. In the latter case, Cr_2O_3 forms a continuous protective ribbon at the interface which stops diffusion of oxygen in the metal and inhibits outward iron diffusion.

Calculations of the oxidation kinetics showed that the oxidation behavior at 500ºC is different from that at 600ºC. The oxide microstructure also evolves with exposure time with a possible change of barrier layer, and consequently, the calculation of the activation energy and of the time rate constant *n* may not be meaningful. The amount of iron needed to form the outer layer is not quite explained by the amount of iron missing from the inner layers, so there is a question of how the outer oxide forms.

Finally, the oxidation behavior of 9CrODS was described as a function of the exposure time for the samples exposed to 600ºC supercritical water. The main aspects of this oxidation behavior are often explained by the presence or absence of Cr_2O_3 which regulates the flow of both oxygen and iron through the oxide layers. For example, the line of pores observed in the oxide layers is explained by the presence of Cr_2O_3 which hinders the replenishment of the vacancies left by the outward diffusion of iron to form the outer layer. Overall, the diffusion of these species is fast through Fe_3O_4, slower through $FeCr_2O_4$ and extremely slow through a continuous film of Cr_2O_3.

ACKNOWLEDGEMENTS

The authors would like to thank Zhonghou Cai and Barry Lai for their help acquiring the data at the APS facility in Argonne National Laboratory. The authors also thank JAEA for providing the 9CrODS used in this study. This study is a DOE-NERI funded project (DE-FC07-06ID14744) and the use of the APS was supported by the DOE, Basic Energy Sciences, Office of Science under Contract No. W-31-109-Eng-38. The authors also thank Andrew Siwy and Jamie Kunkle for their help on this project.

REFERENCES

[1] "A Technology Roadmap for Generation IV Nuclear Energy Systems," GIF-002-00, 2002.

[2] S. Ohtuska, S. Ukai, M. Fujiwara, T. Kaito, and T. Narita, Materials Transactions, 46, (2005), 1.

[3] S. Ukai, S. Mizuta, T. Yoshitake, T. Okuda, M. Fujiwara, S. Hagi, and T. Kobayashi, Journal of Nuclear Materials, 283-287, (2000), 702.

[4] Y. Chen, K. Sridharan, T. R. Allen, and S. Ukai, Journal of Nuclear Materials, 359, (2006), 50.

[5] Y. Chen, K. Sridharan, S. Ukai, and T. R. Allen, Journal of Nuclear Materials, 371, (2007), 118-128.

[6] J. Bischoff, A. T. Motta, and R. J. Comstock, Jourmal of Nuclear Materials, submitted, (2008).

[7] A. D. Siwy, T. E. Clark, and A. T. Motta, Jourmal of Nuclear Materials, submitted, (2008).

[8] L. Tan, M. T. Machut, K. Sridharan, and T. R. Allen, Journal of Nuclear Materials, 371, (2007), 161-170.

[9] L. Tan, Y. Yang, and T. R. Allen, Corrosion Science, 48, (2006), 4234-4242.

[10] L. Tan, Y. Yang, and T. R. Allen, Corrosion Science, 48, (2006), 3123-3138.

[11] P. Ampornrat and G. S. Was, Journal of Nuclear Materials, 371, (2007), 1-17.

[12] Y. Ishikawa, T. Yoshimura, and M. Arai, Vacuum, 47, (1996), 701-704.

[13] A. C. S. Sabioni, A. M. Huntz, F. Silva, and F. Jomard, Materials Science and Engineering A, 392, (2005), 254-261.

[14] A. Motta, A. Yilmazbayhan, M. Gomes da Silva, R. J. Comstock, G. Was, J. Busby, E. Gartner, Q. Peng, Y. H. Jeong, and J. Y. Park, Journal of Nuclear Materials, 371, (2007), 61-75.

[15] C. Wagner, Corrosion Science, 9, (1969), 91-109.

[16] D. P. Whittle and G. C. Wood, Electrochemical Society -- Journal, 114, (1967), 986-993.

[17] J. Robertson, Corrosion Science, 32, (1991), 443-465.

[18] L. Martinelli, F. Balbaud-Célérier, A. Terlain, S. Delpech, G. Santarini, J. Favergeon, G. Moulin, M. Tabarant, and G. Picard, Corrosion Science, 50, (2008), 2523-2536.

[19] L. Martinelli, F. Balbaud-Célérier, A. Terlain, S. Bosonnet, G. Picard, and G. Santarini, Corrosion Science, 50, (2008), 2537-2548.